Improved thermal multiple-relaxation-time lattice Boltzmann model for liquid-vapor phase change

Shengyuan Zhang ⬤,[1] Jun Tang ⬤,[1] Huiying Wu,[1,*] and Rongzong Huang[2]

[1]*School of Mechanical Engineering, Shanghai Jiao Tong University, Shanghai 200240, China*
[2]*School of Energy Science and Engineering, Central South University, Changsha 410083, China*

In this paper, an improved thermal multiple-relaxation-time (MRT) lattice Boltzmann (LB) model is proposed for simulating liquid-vapor phase change. A temperature equation is first derived for liquid-vapor phase change, where the latent heat of vaporization is decoupled with the equation of state. Therefore, the latent heat of vaporization can be arbitrarily specified in practice, which significantly improves the flexibility of the present LB model for liquid-vapor phase change. The Laplacian term of temperature is avoided in the proposed temperature equation and the gradient term of temperature is calculated through a local scheme. To solve the temperature equation accurately and efficiently, an improved MRT LB equation with nondiagonal relaxation matrix is developed. The implicit calculation of the temperature, caused by the source term and encountered in previous works, is avoided by approximating the source term with its value at the previous time step. As demonstrated by numerical tests, the results by the present LB model agree well with analytical results, experimental results, or the results by the finite difference method where the fourth-order Runge-Kutta method is employed to implement the discretization of time.

I. INTRODUCTION

Liquid-vapor phase change processes are of great importance in lots of industrial systems such as power plants [1,2], fluidized beds [3,4], fuel cells [5,6], etc. Related phenomena include the development of moving phase interface and the absorption or release of latent heat. Mathematical modeling of such phenomena remains one of the challenging problems because of the complex boundary conditions and varied thermophysical properties. Recently, the lattice Boltzmann (LB) method originated from the lattice-gas automata [7,8] has shown great potential in simulating liquid-vapor phase change phenomena owing to its obvious advantages, such as the mesoscopic kinetic essences, easy boundary treatment, and inherent parallelizable computational property [9]. Significant progress for liquid-vapor phase change problems, including achieving better thermodynamic consistency, larger density ratio, and tunable surface tension, has been made based on the LB method [10–13]. However, accurate and efficient modeling of the thermal energy transmission for liquid-vapor phase change is still a challenge.

Generally, the existing LB models to describe the thermal energy transmission for liquid-vapor phase change, such as the hybrid model [14–16] and the double-distribution-function (DDF) model [17–19], require a temperature equation to capture the development of temperature field. Zhang and Chen [20] derived a temperature equation for liquid-vapor phase change based on the LB method. Later, Hazi and Markus proposed another temperature equation coupled with a nonideal equation of state [21]. Then, based on Hazi and Markus' work, Gong and Cheng proposed an improved tem-

perature equation for liquid-vapor phase change [22]. With this equation, Gong and Cheng successfully simulated the pool boiling curve from natural convection to stable film boiling [23]. Recently, an improved temperature equation based on Gong and Cheng's model was proposed by Li *et al.* [24] to correct the error terms in Gong and Cheng's model. Similar contributions to improving the temperature equation for liquid-vapor phase change were also made in the past few years [25–28]. Although much progress has been made, a general limitation still exists, i.e., the latent heat of vaporization is coupled with the equation of state, which results in less flexibility to control the vaporization rate.

In this work, we proposed an improved thermal MRT LB model for liquid-vapor phase change. In the present model, a temperature equation is first derived where the latent heat of vaporization is decoupled with the equation of state. Therefore, the latent heat of vaporization can be arbitrarily specified in practice, which significantly improves the flexibility of the present LB model for liquid-vapor phase change. The Laplacian term of temperature is eliminated in the present temperature equation and the gradient term of temperature is calculated through a local scheme. Due to the consistency of numerical methods adopted for the velocity and temperature fields, the DDF model is utilized in the present model for liquid-vapor phase change. An improved thermal MRT LB equation with a nondiagonal relaxation matrix is proposed to solve the temperature equation while a pseudopotential LB model is utilized to capture the hydrodynamic behavior for liquid-vapor phase change. Instead of implementing an iteration procedure, the source term is approximated by its value at the previous time step to calculate the macroscopic temperature in the present model. Satisfactory accuracy of this approximation in real applications is demonstrated through

*Corresponding author: whysrj@sjtu.edu.cn

a series of numerical tests. The rest of the present paper is organized as follows. The pseudopotential model is introduced in Sec. II. The improved thermal MRT LB model is proposed in Sec. III. The validation of the present model is performed in Sec. IV. Finally, Sec. V concludes the paper.

II. PSEUDOPOTENTIAL LB MODEL

For the sake of completeness, the pseudopotential model proposed by Huang and Wu [12] is briefly introduced in this section. In this model, the evolution equation for the density distribution function **f** is

$$
\begin{aligned}
&\mathbf{f}(\mathbf{x} + \mathbf{e}\delta_t, t + \delta_t) - \mathbf{f}(\mathbf{x}, t) \\
&= \mathbf{M}^{-1} \left\{ -\mathbf{S}\mathbf{M}[\mathbf{f}(\mathbf{x}, t) - \mathbf{f}^{\text{eq}}(\mathbf{x}, t)] + \left(\mathbf{I} - \frac{\mathbf{S}}{2} \right) \delta_t \mathbf{F}_m(\mathbf{x}, t) \right. \\
&\quad \left. + \mathbf{S}\mathbf{Q}_m(\mathbf{x}, t) \right\},
\end{aligned}
\tag{1}
$$

where $\mathbf{e}$ is the discrete velocity, δ_t is the time step, $\mathbf{M}$ is the transformation matrix, $\mathbf{S}$ is the relaxation matrix, $\mathbf{f}^{\text{eq}}$ is the equilibrium density distribution function, $\mathbf{I}$ is the unit matrix, $\mathbf{F}_m$ is the discrete force term, and $\mathbf{Q}_m$ is the discrete additional term in the moment space.

The equilibrium density distribution function $\mathbf{f}^{\text{eq}}$ in Eq. (1) is given by

$$
f_i^{\text{eq}} = w_i \rho \left[1 + \frac{\mathbf{e}_i \cdot \mathbf{u}}{c_s^2} + \frac{(\mathbf{e}_i \cdot \mathbf{u})^2}{2c_s^4} - \frac{|\mathbf{u}|^2}{2c_s^2} \right],
\tag{2}
$$

where w_i is the weight coefficient in direction i, ρ is the density, $\mathbf{u}$ is the velocity, and c_s is the lattice sound speed.

For the sake of simplicity, the two-dimensional nine-velocity (D2Q9) lattice [29] is used in this work. Therefore, the discrete velocity is given by

$$
\mathbf{e}_i = \begin{cases} c(0, 0)^{\text{T}}, & i = 0, \\ c\{\cos[(i-1)\pi/2], \sin[(i-1)\pi/2]\}^{\text{T}}, & i = 1, 2, 3, 4, \\ \sqrt{2}c\{\cos[(2i-1)\pi/4], \sin[(2i-1)\pi/4]\}^{\text{T}}, & i = 5, 6, 7, 8, \end{cases}
\tag{3}
$$

where $c = \delta_x/\delta_t$ is the lattice speed, and δ_x is the lattice spacing. The transformation matrix is given by [30]

$$
\mathbf{M} = \begin{pmatrix}
1 & 1 & 1 & 1 & 1 & 1 & 1 & 1 & 1 \\
-4 & -1 & -1 & -1 & -1 & 2 & 2 & 2 & 2 \\
4 & -2 & -2 & -2 & -2 & 1 & 1 & 1 & 1 \\
0 & 1 & 0 & -1 & 0 & 1 & -1 & -1 & 1 \\
0 & -2 & 0 & 2 & 0 & 1 & -1 & -1 & 1 \\
0 & 0 & 1 & 0 & -1 & 1 & 1 & -1 & -1 \\
0 & 0 & -2 & 0 & 2 & 1 & 1 & -1 & -1 \\
0 & 1 & -1 & 1 & -1 & 0 & 0 & 0 & 0 \\
0 & 0 & 0 & 0 & 0 & 1 & -1 & 1 & -1
\end{pmatrix}.
\tag{4}
$$

The relaxation matrix can be written as

$$
\mathbf{S} = \text{diag}(s_0, s_e, s_\varepsilon, s_j, s_q, s_j, s_q, s_p, s_p).
\tag{5}
$$

The lattice sound speed is given by $c_s = c/\sqrt{3}$, and the weight coefficient is given by

$$
w_i = \begin{cases} 4/9, & i = 0, \\ 1/9, & i = 1, 2, 3, 4, \\ 1/36, & i = 5, 6, 7, 8. \end{cases}
\tag{6}
$$

The discrete force term $\mathbf{F}_m$ in Eq. (1) can be written as

$$
\begin{aligned}
\mathbf{F}_m = &\left(0, 6\frac{\mathbf{F} \cdot \mathbf{u}}{c^2}, -6\frac{\mathbf{F} \cdot \mathbf{u}}{c^2}, \frac{F_x}{c}, -\frac{F_x}{c}, \frac{F_y}{c}, -\frac{F_y}{c}, \right. \\
&\left. 2\frac{F_x u_x - F_y u_y}{c^2}, \frac{F_x u_y + F_y u_x}{c^2} \right)^{\text{T}},
\end{aligned}
\tag{7}
$$

where $\mathbf{F} = \mathbf{F}_{in} + \mathbf{F}_b$ is the total force, $\mathbf{F}_{in}$ and $\mathbf{F}_b$ are the interaction force and the external force, respectively. The discrete additional term $\mathbf{Q}_m$ in Eq. (1) is obtained from a third-order Chapman-Enskog analysis to achieve a better thermodynamic consistency, which is given by

$$
\begin{aligned}
\mathbf{Q}_m = &\left(0, 3(k_1 + 2k_2)\frac{|\mathbf{F}_{in}|^2}{G\psi^2 c^2}, -3(k_1 + 2k_2)\frac{|\mathbf{F}_{in}|^2}{G\psi^2 c^2}, \right. \\
&\left. 0, 0, 0, 0, k_1\frac{F_{\text{in},x}^2 - F_{\text{in},y}^2}{G\psi^2 c^2}, k_1\frac{F_{\text{in},x} F_{\text{in},y}}{G\psi^2 c^2} \right)^{\text{T}},
\end{aligned}
\tag{8}
$$

where ψ is the pseudopotential function, G is the interaction strength, k_1 and k_2 are two tunable parameters. In the present work, $k_1 = 0$ and $k_2 = 0.178$ are utilized to achieve better thermodynamic consistency. The relationships between the macroscopic and mesoscopic parameters are defined as

$$
\rho = \sum_i f_i,
\tag{9a}
$$

$$
\rho \mathbf{u} = \sum_i \mathbf{e}_i f_i + \frac{\delta_t}{2}\mathbf{F}.
\tag{9b}
$$

In the pseudopotential LB model, the nonideal equation of state and the nonzero surface tension are simultaneously reproduced by the interaction force $\mathbf{F}_{in}$. For the nearest-neighbor interactions on D2Q9 lattice, the interaction force can be expressed as

$$
\mathbf{F}_{in} = -\frac{Gc^2}{c_s^2}\psi(\mathbf{x}) \sum_{i=1}^8 w_i \psi(\mathbf{x} + \mathbf{e}_i \delta_t)\mathbf{e}_i \delta_t.
\tag{10}
$$

With Eq. (10), the nonideal equation of state can be obtained as

$$
p_{\text{EOS}} = \rho c_s^2 + \frac{G\delta_x^2}{2}\psi^2.
\tag{11}
$$

For a prescribed equation of state in real application, the pseudopotential function is inversely calculated by Eq. (11), i.e., $\psi = \sqrt{2(p_{\text{EOS}} - \rho c_s^2)/(G\delta_x^2)}$. In the present work, the

Peng-Robinson equation of state is utilized, which is given by [31]

$$p_{\text{EOS}} = \frac{\rho R T}{1 - b\rho} - \frac{a\theta(T)\rho^2}{1 + 2b\rho - b^2\rho^2},$$ (12)

where R is the gas constant, $\theta(T) = [1 + (0.374\,64 + 1.542\,26\omega - 0.269\,92\omega^2)(1 - \sqrt{T/T_c})]^2$, $a=0.457\,24R^2T_c^2/p_c$, $b = 0.1873RT_c/p_c$, and T is the temperature which is calculated by Eq. (29b) in real simulations (ω is the acentric factor, T_c is the critical temperature, and p_c is the critical pressure). We utilize $a = 1/49$, $b = 2/21$, and $R = 1$ in the present study and choose $\omega = 0.344$. Considering that the pseudopotential LB model is a diffusive interface model, the position of the interface is defined at $\rho = (\rho_l + \rho_v)/2$ in the present work.

III. IMPROVED THERMAL MRT LB MODEL

A. Temperature equation

Generally, the energy equation utilized to describe the thermal energy transmission for fluid can be expressed by [24]

$$\rho T \frac{Ds}{Dt} = \nabla \cdot (\lambda \nabla T) - \Phi,$$ (13)

where T is the temperature, s is the specific entropy, λ is the thermal conductivity, $\Phi = \rho\varsigma(\partial_j u_j)^2 + \rho\nu/2(\partial_j u_i + \partial_i u_j)^2$ is the dissipation function, and ς and ν are the bulk viscosity and kinematic viscosity, respectively. For liquid-vapor phase change, the dissipation function Φ in Eq. (13) can be neglected [21,22,24,26]. Therefore, the energy equation for liquid-vapor phase change is

$$\rho T \frac{Ds}{Dt} = \nabla \cdot (\lambda \nabla T).$$ (14)

To simplify Eq. (14), a thermodynamic relationship is introduced as

$$T ds = de + p dv = de - \frac{p}{\rho^2} d\rho,$$ (15)

where e is the specific internal energy, p is the pressure, and v is the specific volume. The internal energy e in Eq. (15) can be expressed by

$$de = \left(\frac{\partial e}{\partial T}\right)_\rho dT + \left(\frac{\partial e}{\partial \rho}\right)_T d\rho = c_v dT + \left(\frac{\partial e}{\partial \rho}\right)_T d\rho,$$ (16)

where c_v is the specific heat at constant volume.

Inspired by Hu and Liu [32], in the present work, a linear assumption for the last term in Eq. (16) is made to introduce the latent heat of vaporization h_{lv}, which is given by

$$\left(\frac{\partial e}{\partial \rho}\right)_T d\rho = \frac{e_l - e_v}{\rho_l - \rho_v} d\rho = -\frac{h_{lv} - p_s(v_v - v_l)}{\rho_l - \rho_v} d\rho,$$ (17)

where p_s is the saturated pressure, and the subscripts "v" and "l" denote the vapor and liquid phases, respectively. For the sake of simplicity, a parameter $H = [h_{lv} - p_s(v_v - v_l)]/(\rho_l - \rho_v)$ is introduced. Substituting Eqs. (16) and (17) into Eq. (15), it is obtained that

$$T ds = c_v dT - \left(H + \frac{p}{\rho^2}\right) d\rho.$$ (18)

Then, the temperature equation for liquid-vapor phase change can be obtained by substituting Eq. (18) into Eq. (14):

$$\rho c_v (\partial_t T + \mathbf{u} \cdot \nabla T) = \nabla \cdot (\lambda \nabla T) - \rho^2 \left(H + \frac{p}{\rho^2}\right)(\nabla \cdot \mathbf{u}).$$ (19)

Note that the continuity equation $D\rho/Dt = -\rho \nabla \cdot u$ is also utilized to obtain Eq. (19).

In the DDF model, the temperature equation is solved by a thermal LB equation, which requires the temperature equation as a standard convection-diffusion equation [9]. Considering that

$$\frac{1}{\rho c_v} \nabla \cdot (\lambda \nabla T) = \nabla \cdot (\alpha \nabla T) + \frac{(\alpha \nabla T) \cdot [\nabla(\rho c_v)]}{\rho c_v},$$ (20)

where $\alpha = \lambda/(\rho c_v)$ is the thermal diffusivity, Eq. (19) can be rewritten as

$$\partial_t T + \nabla \cdot (\mathbf{u} T) = \nabla \cdot (\alpha \nabla T) + \frac{(\alpha \nabla T) \cdot [\nabla(\rho c_v)]}{\rho c_v}$$
$$+ \left(T - \frac{\rho H}{c_v} - \frac{p}{\rho c_v}\right)(\nabla \cdot \mathbf{u}).$$ (21)

Note that Eq. (21), as a standard convection-diffusion equation, is the temperature equation proposed in this work. Compared with the previous work, the latent heat is decoupled with the equation of state by Eq. (17). In fact, the thermodynamic relationship utilized in the previous work to simplify the energy equation Eq. (14) is [18,22,24,27]

$$T ds = c_v dT + T \left(\frac{\partial p_{\text{EOS}}}{\partial T}\right)_\rho dv.$$ (22)

The term $(\partial p_{\text{EOS}}/\partial T)_\rho$ in Eq. (22) implicitly combines the latent heat and the equation of state, and thus decreases the flexibility to control the vaporization change rate.

Before proceeding further, some comparisons between the present temperature equation [i.e., Eq. (21)] with previous equations are useful. Comparing Eq. (21) with the temperature equation proposed by Gong and Cheng [22], which is given by

$$\partial_t T + \nabla \cdot (\mathbf{u} T) = \nabla \cdot (\alpha \nabla T)$$
$$+ T \left[1 - \frac{1}{\rho c_v}\left(\frac{\partial p_{\text{EOS}}}{\partial T}\right)_\rho\right](\nabla \cdot \mathbf{u}),$$ (23)

it can be found that the term $(\alpha \nabla T) \cdot [\nabla(\rho c_v)]/(\rho c_v)$ in Eq. (21) is unreasonably neglected in Eq. (23). This incorrect treatment in Gong and Cheng's model has been considered as a major reason causing significant inaccuracy for liquid-vapor phase change [24].

A correction model to Gong and Cheng's model is proposed by Li *et al.* [24]. The temperature equation for liquid-vapor phase change in Li *et al.*'s model is [24]

$$\partial_t T + \nabla \cdot (\mathbf{u} T) = \nabla \cdot (k \nabla T) + \frac{1}{\rho c_v} \nabla \cdot (\lambda \nabla T) - \nabla \cdot (k \nabla T)$$
$$+ T \left[1 - \frac{1}{\rho c_v}\left(\frac{\partial p_{\text{EOS}}}{\partial T}\right)_\rho\right](\nabla \cdot \mathbf{u}),$$ (24)

where k is a constant without physical meaning.

The nonphysical constant k in Eq. (24) is utilized to eliminate the error term in Gong and Cheng's model. Comparing the present temperature equation with Eq. (24), it can be found that the nonphysical constant k in Eq. (24) is replaced by the thermal diffusivity coefficient α in Eq. (21), which can avoid the calculation of the Laplacian of temperature [$\nabla(k\nabla T) = k\nabla^2 T$].

B. Improved thermal MRT LB equation

In this section, an improved thermal MRT LB equation with a temperature distribution function **g** is utilized to solve the temperature equation proposed in this work. The evolution

equation for the temperature distribution function is

$$
\mathbf{g}(\mathbf{x} + \mathbf{e}\delta_t, t + \delta_t) - \mathbf{g}(\mathbf{x}, t)
$$
$$
= \mathbf{M}^{-1} \left\{ -\boldsymbol{\Lambda}_g \mathbf{M}[\mathbf{g}(\mathbf{x}, t) - \mathbf{g}^{\mathrm{eq}}(\mathbf{x}, t)] + \left(\mathbf{I} - \frac{\boldsymbol{\Lambda}_g}{2} \right) \delta_t \mathbf{G}_m \right\},
\tag{25}
$$

where $\mathbf{g}^{\mathrm{eq}}$ is the equilibrium temperature distribution function, $\boldsymbol{\Lambda}_g$ is the relaxation matrix for the thermal MRT LB equation, and $\mathbf{G}_m$ is the discrete source term.

To correctly recover the present temperature equation without deviation term, the nondiagonal relaxation matrix proposed by Huang and Wu [33] is utilized:

$$
\boldsymbol{\Lambda}_g = \begin{pmatrix}
s_0 & 0 & 0 & 0 & 0 & 0 & 0 & 0 & 0 \\
0 & s_1 & 0 & 0 & 0 & 0 & 0 & 0 & 0 \\
0 & 0 & s_2 & 0 & 0 & 0 & 0 & 0 & 0 \\
0 & 0 & 0 & s_3 & s_4\left(\frac{s_3}{2} - 1\right) & 0 & 0 & 0 & 0 \\
0 & 0 & 0 & 0 & s_4 & 0 & 0 & 0 & 0 \\
0 & 0 & 0 & 0 & 0 & s_5 & s_6\left(\frac{s_4}{2} - 1\right) & 0 & 0 \\
0 & 0 & 0 & 0 & 0 & 0 & s_6 & 0 & 0 \\
0 & 0 & 0 & 0 & 0 & 0 & 0 & s_7 & 0 \\
0 & 0 & 0 & 0 & 0 & 0 & 0 & 0 & s_8
\end{pmatrix},
\tag{26}
$$

where s_0, s_1, ..., and s_8 are the relaxation factors. The corresponding equilibrium temperature distribution function is chosen as [33]

$$
g_i^{\mathrm{eq}} = \begin{cases}
\frac{5}{9}T, & i = 0, \\
\left(\frac{1}{18} + \frac{\mathbf{u} \cdot \mathbf{e}_i}{3c^2}\right)T, & i = 1, 2, 3, 4, \\
\left(\frac{1}{18} + \frac{\mathbf{u} \cdot \mathbf{e}_i}{12c^2}\right)T, & i = 5, 6, 7, 8.
\end{cases}
\tag{27}
$$

The discrete source term $\mathbf{G}_m$ in Eq. (25) can be described as

$$
\mathbf{G}_m = (\phi, -2\phi, 2\phi, 0, 0, 0, 0, 0, 0)^{\mathrm{T}}
\tag{28}
$$

where $\phi = \frac{(\alpha\nabla T) \cdot [\nabla(\rho c_v)]}{\rho c_v} + (T - \frac{\rho H}{c_v} - \frac{p}{\rho c_v})(\nabla \cdot \mathbf{u})$ is the source term of Eq. (21). The relationships between the macroscopic and mesoscopic parameters are

$$
s_3 = s_5 = \frac{2c_s^2 \delta_t}{2\alpha + c_s^2 \delta_t},
\tag{29a}
$$

$$
T = \sum_i g_i + \frac{\delta_t}{2}\phi.
\tag{29b}
$$

Note that, due to the temperature related terms, such as $(\alpha\nabla T) \cdot [\nabla(\rho c_v)]$, in the source term ϕ, the calculation of the macroscopic temperature via Eq. (29b) becomes implicit. Instead of implementing an iteration procedure, the source term ϕ in Eq. (29b) is approximated by its value at the previous time step in the present model. The applicability and accuracy of such approximation will be numerically validated in Sec. IV.

Considering that the thermal diffusivity coefficient α varies between the liquid and vapor phases, an interpolation algorithm is introduced to determine the relaxation factor. In the present work, the thermal conductivity λ needs to be calcu-

lated first as

$$
\lambda = \lambda_v + \frac{\rho - \rho_v}{\rho_l - \rho_v}(\lambda_l - \lambda_v).
\tag{30}
$$

Then, the thermal diffusivity α is determined by

$$
\alpha = \frac{\lambda}{\rho c_v},
\tag{31}
$$

and the relaxation factor can be obtained by Eq. (29a).

The Chapman-Enskog analysis for the improved thermal MRT LB equation proposed in this section is performed in Appendix. It can be found that the present temperature equation can be correctly recovered from the improved thermal MRT LB equation with no deviation term. Moreover, a local scheme for the gradient of temperature can also be obtained from the Chapman-Enskog analysis, which is given by

$$
\partial_x T = -\frac{s_3}{c_s^2 \delta_t}\left(m_3^{(1)} + \frac{s_4}{2}m_4^{(1)}\right),
\tag{32a}
$$

$$
\partial_y T = -\frac{s_5}{c_s^2 \delta_t}\left(m_5^{(1)} + \frac{s_6}{2}m_6^{(1)}\right),
\tag{32b}
$$

where $\mathbf{m}^{(1)} = \mathbf{M}(\mathbf{g} - \mathbf{g}^{\mathrm{eq}})$ is the first-order moment function. Note that the isotropic central scheme is widely utilized in previous works to calculated the gradient of temperature [9,24], which is given by

$$
\nabla T = \frac{1}{c_s^2 \delta_t} \sum_i w_i T(\mathbf{x} + \mathbf{e}_i)\mathbf{e}_i.
\tag{33}
$$

The coefficient w_i in Eq. (33) depends on the lattice scheme. Since the D2Q9 lattice is adopted in the present work, this coefficient is the same as Eq. (6). Comparing Eq. (33) with Eq. (32), it can be found that extra information from neighbor
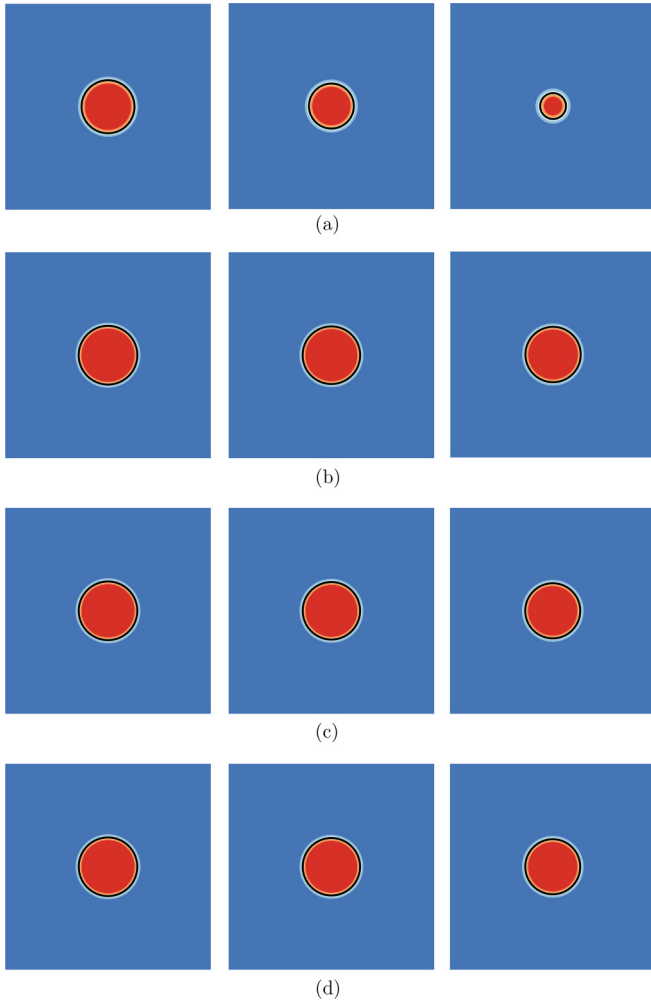
FIG. 1. Simulation of droplet evaporation in open space. Snapshots of the density contours obtained by Gong and Cheng's model [22] (a), Li *et al.*'s model [24] (b), the present LB model (c), and the FDM (d). The snapshots are taken at $t^* = 0.1$, 0.25, and 0.5 (from left to right).

grids is required by Eq. (33). Therefore, with Eq. (32), better locality can be achieved in the present model.

IV. RESULTS AND DISCUSSION

A. Droplet evaporation in open space

Droplet evaporation in open space is a classic benchmark to validate the accuracy of the present LB model for liquid-vapor phase change. In this case, the numerical results are expected to accord with the D2 law which predicts that the square of droplet diameter D decreases linearly with time [15,16,24]:

$$\left(\frac{D}{D_0}\right)^2 = 1 - Kt, \tag{34}$$

where D_0 is the initial droplet diameter, t is the evaporation time, and K is the slope indicating the evaporation rate.

In our simulation, a droplet (initial diameter $D_0 = 60$) at saturated temperature $T_s = 0.86T_c$ is placed at the center of a computational domain ($N_x \times N_y = 200 \times 200$) filled with superheated vapor at uniform temperature T_v. The superheat
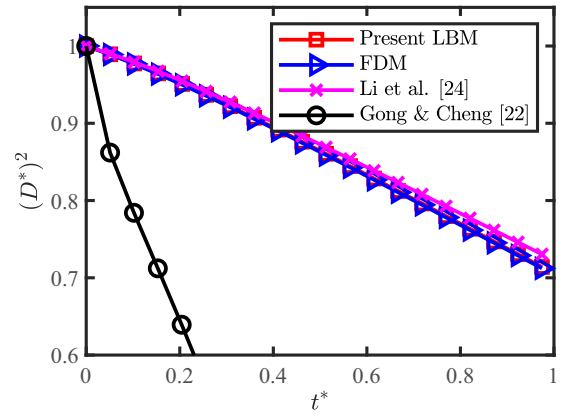

FIG. 2. Simulation of droplet evaporation in open space. Variation of the square of the dimensionless diameter $(D^*)^2$ with the dimensionless time t^*.

of the vapor is set as $T_v - T_s = 0.14T_c$. According to the requirements of the D2 law, the thermal conductivity is chosen as a constant: $\lambda = 1/3$. A constant temperature ($T_b = T_v$) is employed at the boundaries to drive the evaporation process. The total simulation time is set as $t_{\text{total}} = 200\,000\delta_t$.

Note that the present LB model is expected to be able to accurately simulate the liquid-vapor phase change phenomena with a tunable latent heat. To confirm it, the laten heat in the present LB model is first set to the same value as it in the previous LB models proposed by Gong and Cheng [22] and Li *et al.* [24]. As a result, the evaporation rates predicted by the present LB model and the previous LB models should be the same as one another. The latent heat in the previous LB models can be calculated through the method proposed by Gong and Cheng [18], and the result shows that the latent heat is $h_{lv} = 0.1677$ in this case. For comparison, the snapshots of the density contours obtained by the previous LB models and the present LB model are shown in Fig. 1. Meanwhile the variation of the square of the dimensionless diameter $(D^*)^2 = (D/D_0)^2$ with the dimensionless time $t^* = t/t_{\text{total}}$ is displayed in Fig. 2. A finite difference method (FDM), where the fourth-order Runge-Kutta method is employed to implement the discretization of time, is also used to solve Eq. (21), and the numerical results by the FDM are considered in the comparison to validate the present LB model. As the figures show, the evaporation process described by the present LB model is similar to those described by Li *et al.*'s model [24] and the FDM, which indicates the good accuracy of the present LB model. On the other hand, the evaporation rate predicted by Gong and Cheng's model [22] is much larger than the two other LB models and the FDM. The major reason causing the deviation of Gong and Cheng's model [22] is the incorrect treatment for the temperature equation analyzed in Sec. III.

To further validate the ability of the present LB model to control the latent heat and the accuracy of the approximation for the source term in Eq. (29b), the numerical results by the present LB model are further compared with those by the FDM. Two different latent heats, $h_{lv} = 0.19$ and 0.34, are considered. The comparison is shown in Fig. 3. It can be found from Fig. 3 that the results obtained by the present
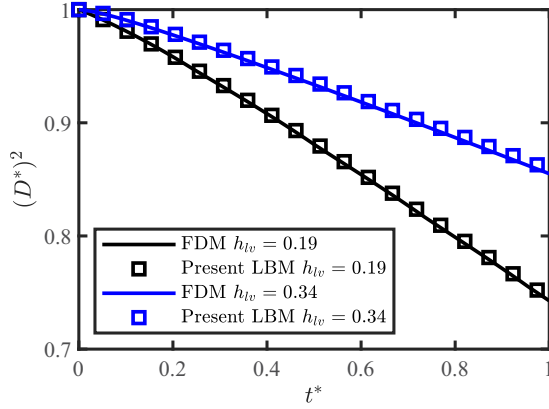
FIG. 3. Simulation of droplet evaporation in open space. Comparison of the present LB model and the FDM.
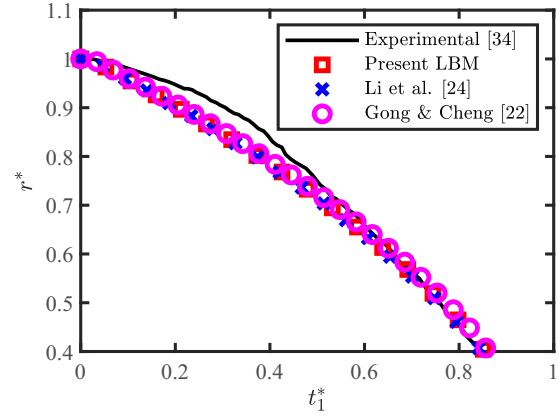

FIG. 4. Simulation of droplet evaporation on a heated substrate. Variation of the dimensionless radius r^* with the dimensionless time t_1^*.

LB model agree well with the results obtained by the FDM, which demonstrates that satisfactory accuracy can be achieved by approximating the source term in Eq. (29b) by its value at the previous time step. It can also be found in Fig. 3 that the results with both latent heats are in good consistency with the D2 law described by Eq. (34) which further validates the ability of the present model to control the evaporation rate. Therefore, in real applications the latent heat of the present model can be flexibly determined through some dimensionless parameters of real phenomena, such as the Jakob number ($\text{Ja} = c_{p,l}\Delta T/h_{lv}$). Note that the previous LB models proposed by Gong and Cheng [22] and Li *et al.* [24] cannot control the latent heat since it is coupled with the equation of state in these models.

As mentioned before, the present LB model requires less computational resource and has better locality than the previous LB models. Therefore, a higher efficiency is expected for the present LB model. To confirm it, a comparison between the run time of the present LB model and the previous LB models is shown in Table I. An OpenMP C++ parallel code is executed using the GNU compiler on a computer with Intel® Xeon® E5-2697 v3 processor (CPU) @ 2.60 GHz base frequency and 128.0 GB shared memory (RAM). The results in Table I show the computational cost per time step for this case. As it can be seen, the present LB model achieves the highest efficiency while Gong and Cheng's model [22] and Li *et al.*'s model [24] have a similar performance.

B. Droplet evaporation on heated surface

Droplet evaporation on a heated surface is another benchmark used to validate the present LB model for liquid-vapor phase change. In this case, the numerical results are compared

TABLE I. Comparison between the computational efficiency of the present and previous LB models. The CPU time (in seconds) per iteration for a 200^2 grid on a shared-memory computer using 12 processors.

	Present model	Gong and Cheng [22]	Li *et al.* [24]
CPU time (s)	3.14×10^{-3}	3.72×10^{-3}	3.62×10^{-3}

with the experimental results obtained by Dash and Garimella [34]. In their experiment, a small droplet is heated on a hydrophobic substrate with an initial contact angle of 120°. The environmental temperature is $21 \pm 0.5\,°\text{C}$ while the substrate temperature is $40\,°\text{C}$. In the simulations, we set a computation domain with $N_x \times N_y = 300 \times 150$. A droplet of diameter $D_0 = 70$ at temperature $T_s = 0.86T_c$ is initially located on a heated surface surrounded by saturated vapor. To agree with the experiment, the Jakob number [$\text{Ja} = c_{p,l}(T_w - T_s)/h_{lv}$, where T_w is the wall temperature] in the simulations is set as the same as the Jakob number in the experiment which is $\text{Ja} = 0.036$ in this case. The Dirichlet boundary condition for temperature and no-slip boundary condition for velocity are applied at the bottom boundary, while other boundaries are considered as no-gradient boundaries for both temperature and velocity.

The present LB model is first compared with the previous LB models proposed by Gong and Cheng [22] and Li *et al.* [24]. Therefore, the latent heat is set as $h_{lv} = 0.1677$ to be consistent with the previous LB models and the corresponding wall temperature is set as $T_w = 0.8925T_c$. The variation of the dimensionless radius $r^* = r/r_0$ with the dimensionless time $t_1^* = t/t_0$ (r_0 and t_0 are the initial radius and the total evaporation time, respectively) is displayed in Fig. 4. Note that in our simulation a large transition of the dimensionless radius r^* caused by the initial-condition effect is observed at the beginning of the evaporation process. Therefore, the comparison is considered after the initial-condition effect is ignorable. The errors between the numerical results and experimental results are shown in Fig. 5, which is defined by

$$\text{Error} = |r^*_{\text{numerical}} - r^*_{\text{experimental}}|. \quad (35)$$

Considering that the interface is diffusive in the LB model, the radius of the droplet at the final evaporation stage will not be considered to guarantee the accuracy of the tracked position of phase interface. As Figs. 4 and 5 show, the results obtained by the present LB model and the previous LB models agree well with the experimental results. Note that in Fig. 4 the dimensionless radius r^* and the dimensionless time t_1^* are utilized in the comparison where the dimensionless time
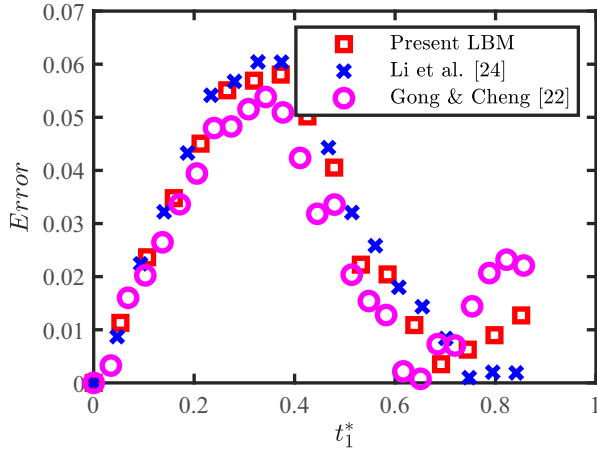
FIG. 5. Simulation of droplet evaporation on a heated substrate. The errors between the numerical results and experimental results.

FIG. 7. Simulation of droplet evaporation on a heated substrate. Comparison of the present LB model with FDM.

t_1^* is normalized by the total evaporation time t_0. However, the total evaporation time predicted by each model is different. Therefore, the present LB model is further compared with the previous LB models with another dimensionless time t_2^* which is normalized by a constant total simulation time $t_{\text{total}} = 130\,000\delta_t$ ($t_2^* = t/t_{\text{total}}$). The results by the FDM are also considered in this comparison shown in Fig. 6. It can be found that the evaporation process described by the present model agrees well with the evaporation processes described by Li *et al.*'s model [24] and the FDM, while a larger deviation can be observed for Gong and Cheng's model [22].

Then, the present LB model is compared with the FDM to validate the accuracy of the approximation for the source term in Eq. (29b) and the ability of the present LB model to control latent heat. For this comparison, two latent heats $h_{lv} = 0.19$ and 0.27 are considered and the corresponding Jakob numbers are 0.0031 and 0.0022, respectively. The variation of the dimensionless radius r^* with the dimensionless time $t_2^* = t/t_{\text{total}}$ is shown in Fig. 7. It can be observed from Fig. 7 that the results obtained by the present LB model are in good

agreement with the results obtained by the FDM for both two different latent heats, which further demonstrates the accuracy of the approximation for the source term in Eq. (29b). It can be also found in Fig. 7 that the vaporization rates are well controlled by the present model with the tunable latent heat.

C. Bubble nucleation and departure

In this section, numerical simulations are carried out for bubble nucleation and departure involved in nucleate boiling to validate the present LB model. The simulation domain is set as $N_x \times N_y = 150 \times 300$ filled with saturated water at $T_s = 0.86T_c$. The corresponding surface tension of the case is $\sigma_{lv} = 0.0546$, which can be obtained through the Laplace's law for the sphere bubble ($\sigma_{lv} = \Delta p \times R$). For simplicity, the thermal diffusivity and specific heat are set as constant: $\alpha = 0.1$ and $c_v = 5$, respectively. A higher temperature $T_w = 1.25T_c$ is applied to the center five grids of the bottom wall while an adiabatic boundary condition is applied to the rest of the bottom wall. The equilibrium contact angle is set as 45°. To simulate the bubble departure, a buoyant
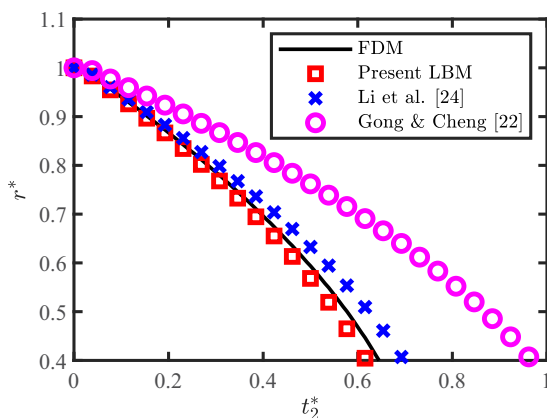

FIG. 6. Simulation of droplet evaporation on a heated substrate. Variation of the dimensionless radius r^* with the dimensionless time t_2^*.
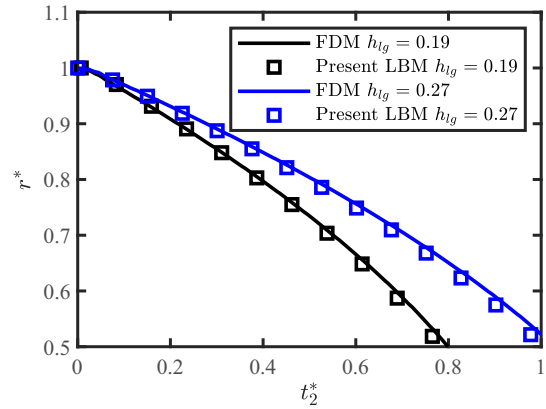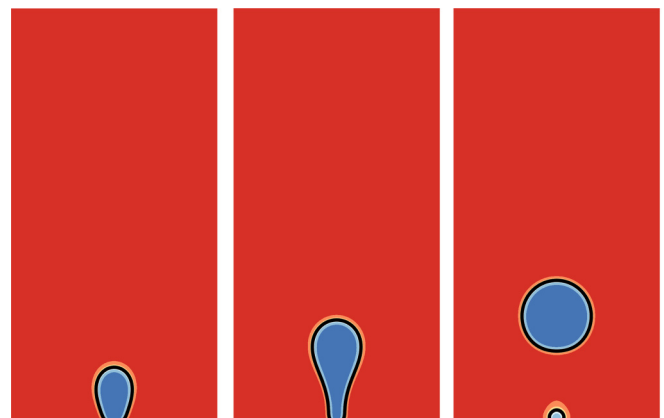

FIG. 8. Simulation of bubble nucleation and departure ($g = 2.75 \times 10^{-5}$, $h_{lv} = 0.120$). Snapshot of the density contours. The snapshots are taken at $t = 140\,000\delta_t$, $t = 146\,000\delta_t$, $t = 148\,500\delta_t$ (from left to right).
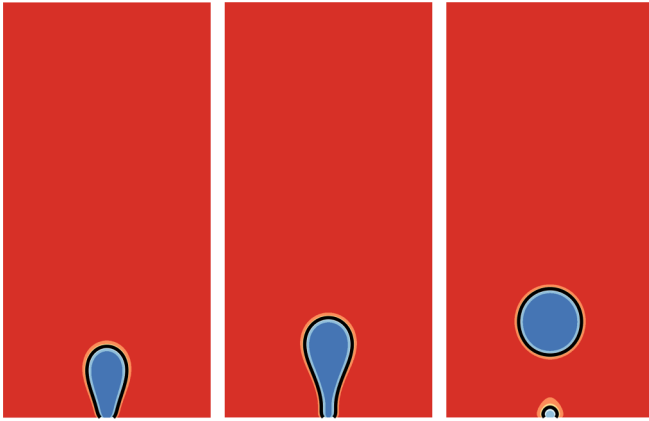
FIG. 9. Simulation of bubble nucleation and departure ($g = 2.75 \times 10^{-5}$, $h_{lv} = 0.145$). Snapshot of the density contours. The snapshots are taken at $t = 161\,000\delta_t$, $t = 164\,000\delta_t$, $t = 166\,000\delta_t$ (from left to right).

force defined by $\mathbf{F}_b = (\rho - \rho_{ave})\mathbf{g}$ is applied, where ρ_{ave} is the average density in the domain and $\mathbf{g} = (0, -g)$ is the gravity acceleration. To further validate the ability of the present LB model to control the latent heat, two different
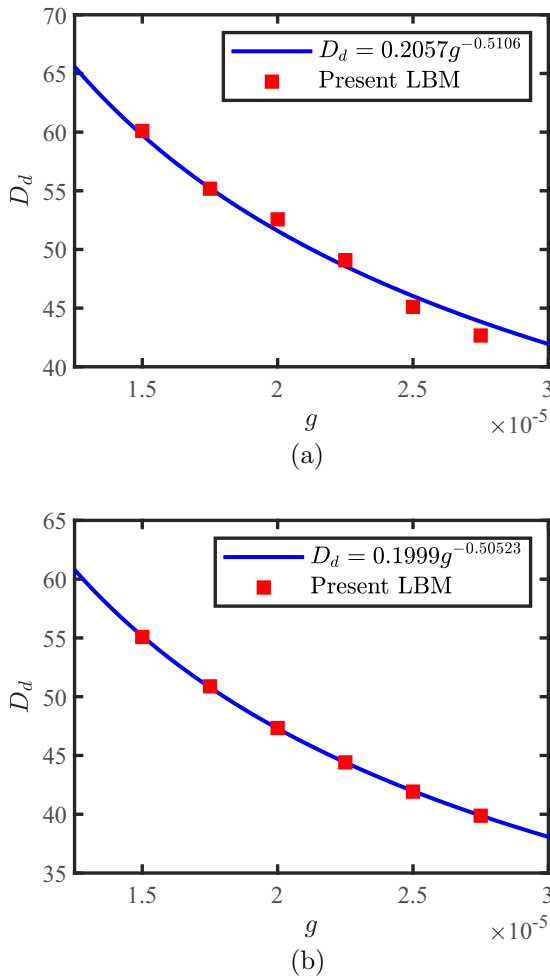

(a)

(b)

FIG. 10. Simulations of bubble nucleation and departure. Variation of detachment bubble diameter with gravity acceleration. $h_{lv} = 0.120$ (a) and $h_{lv} = 0.145$ (b).

latent heats $h_{lv} = 0.120$ and 0.145 are considered in this case, where the corresponding Jakob numbers are 0.592 and 0.490, respectively.

The snapshots of the density contours obtained by the present LB model with latent heats $h_{lv} = 0.120$ and 0.145 are shown in Figs. 8 and 9, respectively. It can be found that a small bubble is first formed at the center of the wall. Then, a neck caused by the buoyancy gradually appears and finally breaks. These processes of bubble growth and detachment observed from Figs. 8 and 9 agree well with those described in the previous works [22–24]. It can be found that the bubble detachment time with larger latent heat $h_{lv} = 0.145$ will be longer than that with $h_{lv} = 0.120$.

Another expected result to validate the present LB model for liquid-vapor phase change is the relationship between detachment bubble diameter and gravity acceleration (i.e., $D_d \propto g^{-0.5}$) [22,24,26,27]. Therefore, the simulations of bubble nucleation and departure are also carried out under a series of gravity acceleration. The variation of the detachment bubble diameter with the gravity acceleration is shown in Fig. 10. The results obtained by the present LB model are compared with a fitted line. From Fig. 10, it can be found that the relationships between the detachment bubble diameter and the gravity acceleration are well predicted by the present LB model for two different latent heats, which further demonstrates the accuracy of the present LB model with different latent heats.

V. CONCLUSION

In this work, an improved thermal MRT LB model for liquid-vapor phase change is proposed. For the velocity field, the pseudopotential model proposed by Huang and Wu [12] is utilized to capture the hydrodynamic behavior. For the temperature field, a temperature equation is first derived for liquid-vapor phase change, where the latent heat is decoupled with the equation of state by a linear assumption described in Eq. (17), which improves the flexibility of the present model to control the vaporization rate. The error terms in the previous model are eliminated in the present model. What's more, the Laplacian term of temperature is not needed in the present temperature equation and the gradient term of temperature is calculated through a local scheme. To solve the temperature equation accurately and efficiently, an improved thermal MRT equation with nondiagonal relaxation matrix is developed. The implicit calculation of temperature caused by the source term is avoided by approximating the source term in Eq. (29b) by its value at the previous time step. Numerical tests demonstrate that the liquid-vapor phase change phenomena can be accurately simulated by the present LB model with a tunable latent heat. It is found that a higher computation efficiency is achieved by the present LB model.

APPENDIX: CHAPMAN-ENSKOG ANALYSIS OF EQ. (25)

Applying the Taylor series expansion to Eq. (25), we have

$$(\mathbf{I}\partial_t + \mathbf{D})\mathbf{m} + \frac{\delta_t}{2}(\mathbf{I}\partial_t + \mathbf{D})^2\mathbf{m} + O(\delta_t^2)$$

$$= -\frac{\boldsymbol{\Lambda}_g}{\delta_t}(\mathbf{m} - \mathbf{m}^{eq}) + \left(\mathbf{I} - \frac{\boldsymbol{\Lambda}_g}{2}\right)\mathbf{G}_m, \qquad (A1)$$

where $\mathbf{D} = \mathbf{M}[\text{diag}(\mathbf{e}_0 \cdot \nabla, \ldots, \mathbf{e}_8 \ldots \nabla)]\mathbf{M}^{-1}$, $\mathbf{m} = \mathbf{Mg}$ is the moment function, and $\mathbf{m}^{eq} = \mathbf{Mg}^{eq}$ is the equilibrium moment function. By introducing the following Chapman-Enskog expansions:

$$\partial_t = \varepsilon\partial_{t1} + \varepsilon^2\partial_{t2}, \quad \nabla = \varepsilon\nabla_1,$$

$$\mathbf{m} = \sum_{n=0}^{+\infty}\varepsilon^n\mathbf{m}^{(n)}, \quad \phi = \varepsilon\phi^{(1)}, \quad \mathbf{G}_m = \varepsilon\mathbf{G}_m^{(1)}, \quad (A2)$$

and substituting them into Eq. (A1), Eq. (A1) can be rewritten in the consecutive orders of the small expansion parameter ε:

$$\varepsilon^0: \ \mathbf{m}^{(0)} = \mathbf{m}^{eq}, \qquad (A3a)$$

$$\varepsilon^1: (\mathbf{I}\partial_{t1} + \mathbf{D}_1)\mathbf{m}^{(0)} - \mathbf{G}_m = -\frac{\boldsymbol{\Lambda_g}}{\delta_t}\left(\mathbf{m}^{(1)} + \frac{\delta_t}{2}\mathbf{G}_m\right), \qquad (A3b)$$

$$\varepsilon^2: \partial_{t2}\mathbf{m}^{(0)} + (\mathbf{I} + \mathbf{D}_1)\left(\mathbf{I} - \frac{\boldsymbol{\Lambda}_g}{2}\right)\left(\mathbf{m}^{(1)} + \frac{\delta_t}{2}\mathbf{G}_m^{(1)}\right)$$

$$= -\frac{\boldsymbol{\Lambda}_g}{\delta_t}\mathbf{m}^{(2)}. \qquad (A3c)$$

Considering Eqs. (29b) and (A2), it can be obtained that [35]

$$m_0^{(1)} + \frac{\delta_t}{2}\phi^{(1)} = 0, \quad m_0^{(n)} = 0(\forall n \geqslant 2). \qquad (A4)$$

Then, according to Eq. (A3b), we have

$$\partial_{t1}T + \nabla_1 \cdot (\mathbf{u}T) = \phi^{(1)}, \qquad (A5a)$$

$$\partial_{t1}(Tu_x) + c_s^2\partial_{x1}T = -\frac{s_3}{\delta_t}m_3^{(1)} + \left(1 - \frac{s_3}{2}\right)\frac{s_4}{\delta_t}m_4^{(1)}, \qquad (A5b)$$

$$\partial_{t1}(Tu_y) + c_s^2\partial_{y1}T = -\frac{s_5}{\delta_t}m_5^{(1)} + \left(1 - \frac{s_5}{2}\right)\frac{s_6}{\delta_t}m_6^{(1)}, \qquad (A5c)$$

$$-\partial_{t1}(Tu_x) = -\frac{s_4}{\delta_t}m_4^{(1)}, \qquad (A5d)$$

$$-\partial_{t1}(Tu_y) = -\frac{s_6}{\delta_t}m_6^{(1)}. \qquad (A5e)$$

From Eq. (A3c), it is obtained that

$$\partial_{t2}T + \nabla_1 \cdot \begin{bmatrix} \left(1 - \frac{s_3}{2}\right)\left(m_3^{(1)} + \frac{s_4}{2}m_4^{(1)}\right) \\ \left(1 - \frac{s_5}{2}\right)\left(m_5^{(1)} + \frac{s_6}{2}m_6^{(1)}\right) \end{bmatrix} = 0. \qquad (A6)$$

To simplify Eq. (A6), the following relations are introduced by adding Eqs. (A5d) and (A5e) to Eqs. (A5b) and (A5c), respectively:

$$c_s^2\partial_{x1}T = -\frac{s_3}{\delta_t}\left(m_3^{(1)} + \frac{s_4}{2}m_4^{(1)}\right), \qquad (A7a)$$

$$c_s^2\partial_{y1}T = -\frac{s_5}{\delta_t}\left(m_5^{(1)} + \frac{s_6}{2}m_6^{(1)}\right). \qquad (A7b)$$

Substituting Eqs. (A7a) and (A7b) into Eq. (A6), we have

$$\partial_{t2}T = \nabla_1 \cdot \begin{bmatrix} \left(\frac{1}{s_3} - \frac{1}{2}\right)\delta_t c_s^2\partial_{x1}T \\ \left(\frac{1}{s_5} - \frac{1}{2}\right)\delta_t c_s^2\partial_{y1}T \end{bmatrix}. \qquad (A8)$$

Considering Eq. (29a), Eq. (A8) can be further simplified as

$$\partial_{t2}T = \nabla_1 \cdot (\alpha\nabla_1 T). \qquad (A9)$$

Adding Eq. (A9) to Eq. (A5a), we have

$$\partial_t T + \nabla \cdot (\mathbf{u}T) = \nabla \cdot (\alpha\nabla T) + \phi. \qquad (A10)$$

Obviously, Eq. (A10) is the same as Eq. (21), which proves that the targeted temperature equation proposed in the present work can be correctly recovered from the thermal MRT LB equation [i.e., Eq. (25)] with no deviation term. Note that the local algorithm described in Eq. (32) can be obtained by Eq. (A7).

[1] F.-B. Cheung, F. A. Sohag, and M. P. Riley, Development of a downward-facing nucleate boiling correlation for thermal hydraulics analysis, Exp. Therm. Fluid Sci. **120**, 110256 (2021).

[2] S. V. Ivanov and V. I. Gorburov, Behavior of impurities in the volume of boiling medium in the equipment of nuclear and thermal power stations, Therm. Eng. **57**, 447 (2010).

[3] X. Ren, J. Zheng, S. Khellil, and A.-I. Michael, Flow boiling heat transfer in circulating fluidized bed, Front. Energy Power Eng. China **3**, 85 (2009).

[4] M. Arumemi-Ikhide, K. Sefiane, G. Duursma, and D. Glass, Investigation of flow boiling in circulating three-phase fluidised bed, Chem. Eng. Sci. **63**, 896 (2008).

[5] Z. Qi and A. Kaufman, Enhancement of PEM fuel cell performance by steaming or boiling the electrode, J. Power Sources **109**, 227 (2002).

[6] U. Soupremanien, S. Le Person, M. Favre-Marinet, and Y. Bultel, Tools for designing the cooling system of a proton exchange membrane fuel cell, Appl. Therm. Eng. **40**, 161 (2012).

[7] U. Frisch, B. Hasslacher, and Y. Pomeau, Lattice-Gas Automata for the Navier-Stokes Equation, Phys. Rev. Lett. **56**, 1505 (1986).

[8] G. R. McNamara and G. Zanetti, Use of the Boltzmann Equation to Simulate Lattice-Gas Automata, Phys. Rev. Lett. **61**, 2332 (1988).

[9] Q. Li, K. H. Luo, Q. J. Kang, Y. L. He, Q. Chen, and Q. Liu, Lattice boltzmann methods for multiphase flow and phase-change heat transfer, Prog. Energy Combust. Sci. **52**, 62 (2016).

[10] Q. Li, K. H. Luo, and X. J. Li, Lattice boltzmann modeling of multiphase flows at large density ratio with an improved pseudopotential model, Phys. Rev. E **87**, 053301 (2013).

[11] Q. Li and K. H. Luo, Achieving tunable surface tension in the pseudopotential lattice boltzmann modeling of multiphase flows, Phys. Rev. E **88**, 053307 (2013).

[12] R. Huang and H. Wu, Third-order analysis of pseudopotential lattice boltzmann model for multiphase flow, J. Comput. Phys. **327**, 121 (2016).

[13] R. Huang, H. Wu, and N. A. Adams, Lattice boltzmann model with self-tuning equation of state for multiphase flows, Phys. Rev. E **99**, 023303 (2019).

[14] Q. Li, Q. J. Kang, M. M. Francois, Y. L. He, and K. H. Luo, Lattice boltzmann modeling of boiling heat transfer: the boiling curve and the effects of wettability, Int. J. Heat Mass Transf. **85**, 787 (2015).

[15] Q. Li, Q. J. Kang, M. M. Francois, and A. J. Hu, Lattice boltzmann modeling of self-propelled leidenfrost droplets on ratchet surfaces, Soft Matter **12**, 302 (2016).

[16] S. Zheng, F. Eimann, T. Fieback, G. Xie, and U. Gross, Numerical investigation of convective dropwise condensation flow by a hybrid thermal lattice boltzmann method, Appl. Therm. Eng. **145**, 590 (2018).

[17] L. Biferale, P. Perlekar, M. Sbragaglia, and F. Toschi, Convection in Multiphase Fluid Flows Using Lattice Boltzmann Methods, Phys. Rev. Lett. **108**, 104502 (2012).

[18] S. Gong and P. Cheng, Lattice boltzmann simulation of periodic bubble nucleation, growth and departure from a heated surface in pool boiling, Int. J. Heat Mass Transf. **64**, 122 (2013).

[19] A. Márkus and G. Házi, Simulation of evaporation by an extension of the pseudopotential lattice boltzmann method: A quantitative analysis, Phys. Rev. E **83**, 046705 (2011).

[20] R. Zhang and H. Chen, Lattice boltzmann method for simulations of liquid-vapor thermal flows, Phys. Rev. E **67**, 066711 (2003).

[21] G. Hazi and A. Markus, On the bubble departure diameter and release frequency based on numerical simulation results, Int. J. Heat Mass Transf. **52**, 1472 (2009).

[22] S. Gong and P. Cheng, A lattice boltzmann method for simulation of liquid–vapor phase-change heat transfer, Int. J. Heat Mass Transf. **55**, 4923 (2012).

[23] S. Gong and P. Cheng, Lattice boltzmann simulations for surface wettability effects in saturated pool boiling heat transfer, Int. J. Heat Mass Transf. **85**, 635 (2015).

[24] Q. Li, P. Zhou, and H. J. Yan, Improved thermal lattice boltzmann model for simulation of liquid-vapor phase change, Phys. Rev. E **96**, 063303 (2017).

[25] C. Zhang, P. Cheng, and W. J. Minkowycz, Lattice boltzmann simulation of forced condensation flow on a horizontal cold surface in the presence of a non-condensable Gas, Int. J. Heat Mass Transf. **115**, 500 (2017).

[26] W.-Z. Fang, L. Chen, Q.-J. Kang, and W.-Q. Tao, Lattice boltzmann modeling of pool boiling with large liquid-gas density ratio, Int. J. Therm. Sci. **114**, 172 (2017).

[27] S. Wu, C. Yu, F. Yu, and Y. Chen, Lattice boltzmann simulation of co-existing boiling and condensation phase changes in a confined micro-space, Int. J. Heat Mass Transf. **126**, 773 (2018).

[28] F. Qin, L. Del Carro, A. Mazloomi Moqaddam, Q. Kang, T. Brunschwiler, D. Derome, and J. Carmeliet, Study of non-isothermal liquid evaporation in synthetic micro-pore structures with hybrid lattice boltzmann model, J. Fluid Mech. **866**, 33 (2019).

[29] Y. H. Qian, D. D'Humières, and P. Lallemand, Lattice BGK models for navier-stokes equation, Europhys. Lett. **17**, 479 (1992).

[30] P. Lallemand and L.-S. Luo, Theory of the lattice boltzmann method: dispersion, dissipation, isotropy, galilean invariance, and stability, Phys. Rev. E **61**, 6546 (2000).

[31] P. Yuan and L. Schaefer, Equations of state in a lattice boltzmann model, Phys. Fluids **18**, 042101 (2006).

[32] A. Hu and D. Liu, A superheat degree driven liquid-vapor phase-change lattice boltzmann model, Int. J. Heat Mass Transf. **136**, 674 (2019).

[33] R. Huang and H. Wu, A modified multiple-relaxation-time lattice boltzmann model for convection–diffusion equation, J. Comput. Phys. **274**, 50 (2014).

[34] S. Dash and S. V. Garimella, Droplet evaporation on heated hydrophobic and superhydrophobic surfaces, Phys. Rev. E **89**, 042402 (2014).

[35] R. Huang and H. Wu, Phase interface effects in the total enthalpy-based lattice boltzmann model for solid–liquid phase change, J. Comput. Phys. **294**, 346 (2015).